

Distribution of grain boundaries in aluminum as a function of five macroscopic parameters

David M. Saylor¹, Bassem S. El Dasher², Anthony D. Rollett, Gregory S. Rohrer^{*}

Department of Materials Science and Engineering, Carnegie Mellon University, Pittsburgh, PA 15213-3890, USA

Received 31 March 2004; accepted 22 April 2004

Available online 18 May 2004

Abstract

The grain boundary character distribution in commercially pure Al has been measured as a function of lattice misorientation and boundary plane orientation. The results demonstrate a tendency to terminate grain boundaries on low index planes with relatively low surface energies and large interplanar spacings. The most frequently observed grain boundary plane orientation is (111). However, there are also instances where boundaries terminated by higher index planes have significant populations. For example, certain twist configurations on {11 w } planes, which correspond to symmetric [110] tilt boundaries, also have relatively high populations. The population of symmetric [110] tilt boundaries exhibits an inverse relationship with previously measured energies.

© 2004 Acta Materialia Inc. Published by Elsevier Ltd. All rights reserved.

Keywords: Aluminum; Grain boundaries; Microstructure; Electron backscattering patterns; Texture

1. Introduction

With the emergence of high speed electron back scattered diffraction pattern mapping systems, it has become possible to quantitatively evaluate the grain boundary character distribution in polycrystalline specimens over all five macroscopic degrees of freedom. Recent results have indicated that at fixed lattice misorientations, there is significant anisotropy in the distribution of grain boundary planes and that in general, the same low index surfaces that appear on equilibrium crystal shapes and growth habits of crystals also dominate the distribution of internal grain surfaces [1–3]. Furthermore, there is an inverse correlation between the energy of a grain boundary and its population in the distribution [4]. The purpose of this paper is to examine the grain boundary character distribution in a cubic

close-packed metal (commercially pure Al, alloy 1050) and to determine if the observations can be correlated with experimental measurements of the surface and grain boundary energies.

2. Methods

The specimen was cut from a sheet of aluminum alloy 1050 which had been cold rolled to approximately 80% reduction of thickness. The sample was annealed at 400 °C in dry, flowing nitrogen for 60 min to create an equiaxed microstructure with a grain size of approximately 23 μm. Following the heat treatment, the sample surface was wet ground and then electropolished at 20 V, with a current density of ~0.26 A/cm² using a solution consisting of 73% ethanol, 7.5% perchloric acid, 9.5% ethylene glycol monobutyl ether and 10% distilled water.

Crystal orientation maps on a planar section were obtained using an EBSD mapping system (TexSEM Laboratories, Inc.) integrated with a scanning electron microscope (Phillips XL40 FEG). Orientations were recorded at intervals of 2 μm on a hexagonal grid.

^{*} Corresponding author. Tel.: +1-412-268-2696; fax: +1-412-268-3113.

E-mail address: gr20@andrew.cmu.edu (G.S. Rohrer).

¹ Present address: U.S.F.D.A., 12725 Twinbrook Parkway, Rockville, MD 20852, USA.

² Present address: Lawrence Livermore National Laboratory, University of California, P.O. Box 808, Livermore, CA 94511, USA.

Individual maps with areas less than or equal to 1 mm^2 were recorded at a single stage position. Data from multiple areas were combined so that the orientation maps covered an area of 5.6 mm^2 . To divide the orientation maps into grains with a constant orientation, areas with similar orientations were first dilated so that the smallest grain consisted of at least eight contiguous data points, and then the mean orientation of each grain was determined and assigned to all the points within the contiguous area [5].

These data were used to determine the grain boundary character distribution, $k(\Delta g; n)$, which is defined as the relative areas of distinguishable grain boundaries characterized by their lattice misorientation (Δg) and boundary plane orientation (n). The grain boundary character distribution is measured in multiples of a random distribution (MRD); values greater than one indicate planes observed more frequently than expected in a random distribution. The orientation maps described above provide us with four of the five parameters necessary to specify the distribution: the three misorientation parameters and one of the two parameters needed to describe the orientation of the grain boundary plane. Here we use a previously described stereological procedure for extracting the grain boundary character distribution from these data [6].

The main requirement for the stereological procedure is that a sufficient number of grain boundary traces (lines of intersection between a grain boundary and the surface) be characterized with respect to their lattice misorientation and orientation within the section plane. While the actual plane orientation for each trace is never known, it must be in the zone of the trace and if enough traces are observed from symmetrically indistinguishable bicrystals, then the probability that certain grain boundary planes appear in the microstructure can be defined. The number of grain boundary traces needed to generate a grain boundary character distribution depends on the crystal symmetry, the resolution of the five angular parameters, and the desired accuracy. In the original description of this technique, it was found that if the angular parameters in a cubic system are resolved at 10° , then 50,000 grain boundary traces are sufficient to determine $k(\Delta g; n)$ so that the error in k for 95% of all the grain boundary types is less than 0.5 MRD [6]. In the present case, more than 57,000 traces bounding more than 11,000 distinct grains were analyzed.

In the current paper, the grain boundary traces were extracted from the orientation maps using a procedure described by Wright and Larsen [7]. The grain boundary character distribution, $k(\Delta g; n)$, is parameterized and discretized as described in our previous work, and therefore has a resolution of approximately 10° [1]. It should be noted that the stereological procedure used to extract $k(\Delta g; n)$ assumes that random sections of bicrystals are sampled. In other words, it is assumed that

the sample has no texture. In fact, the samples examined here exhibited weak grain orientation texture. Grains with $[112]$ poles perpendicular to the sample surface occurred with a frequency of 2.4 MRD and grains with $[100]$ and $[110]$ poles perpendicular to the sample surface occurred with a frequency of approximately 1.5 MRD. To determine the effect of this orientation bias on the stereological extraction of $k(\Delta g; n)$, a test data set was constructed with the same orientation texture and a known (hypothetical) grain boundary character distribution. The grain boundary character distribution extracted from the textured test data had errors that were similar in size to that extracted from untextured test data. We therefore conclude that the texture of the sample did not significantly influence the results.

3. Results

If the grain boundary character distribution is taken to be a function of misorientation alone, then $k(\Delta g)$ can be examined in a three dimensional space. The dominant feature in the misorientation distribution is an enhancement in the population of low misorientation angle grain boundaries. The distribution of high angle boundaries, (those boundaries with misorientations greater than 10°) averaged over all values of n is plotted in Rodrigues–Frank [8] space in Fig. 1. Here, each Δg is denoted by a unique vector with a direction parallel to the common axis of misorientation and a magnitude that is proportional to the tangent of one half of the disorientation angle. In Fig. 1, the r_1 direction is parallel to $[100]$ and the individual plots show slices through the three dimensional space perpendicular to $[001]$ (r_3). The distribution shows a weak preference for high angle misorientations about $[110]$ and the $\Sigma 3$ misorientation, $k(60^\circ/[111])$. The distribution of grain boundary planes, $k(n)$, can also be examined, independent of the misorientation parameters. This distribution is plotted in Fig. 2. Note that the grain boundary plane distribution is plotted in the crystal reference frame. The maximum of the distribution occurs at the $\{111\}$ positions and the minimum occurs at $\{100\}$ positions.

We can also examine the distribution of grain boundary planes at specific misorientations, $k(n|\Delta g)$. Here, the misorientations are selected according to the axis–angle convention by specifying the common axis of rotation $[uvw]$, and an angle about that axis, α . After fixing the misorientation, $k(n|\alpha=[uvw])$ is then plotted on a stereographic projection. Examples for three high coincidence lattice misorientations about the $[111]$ axis ($5^\circ \sim \Sigma 1$, $38^\circ = \Sigma 7$, and $60^\circ = \Sigma 3$) are shown in Fig. 3. A schematic in Fig. 3(a) shows the reference frame for the projection and indicates the locations of the plane normals associated with twist boundaries (parallel to the $[111]$ misorientation axis) and the normals associated

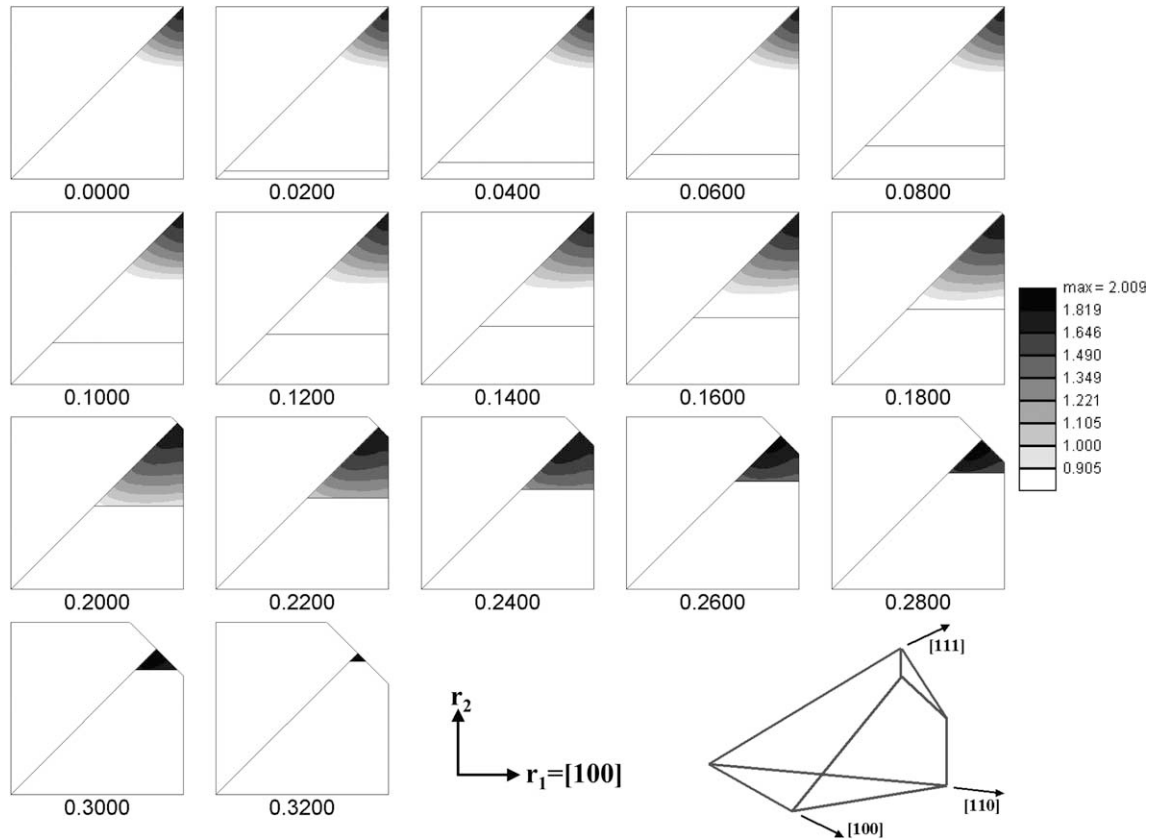


Fig. 1. A plot of $k(\Delta g)$, the distribution of grain boundary misorientations in commercially pure aluminum after annealing for 60 min at 400 C. Planar sections of the three dimensional fundamental zone in Rodrigues–Frank space, perpendicular to the $[001]$ axis, are plotted with the vertical coordinate below each section. In the lower right hand corner, an oblique projection of the three dimensional fundamental zone is shown.

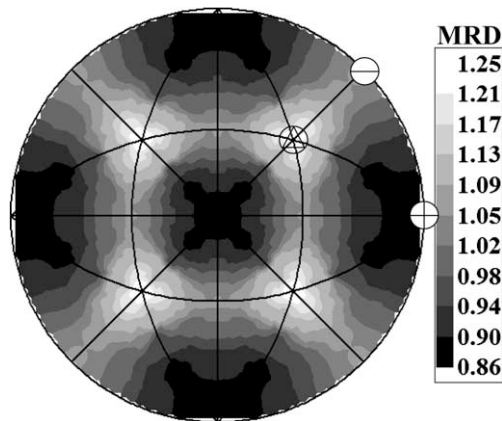


Fig. 2. A plot of $k(n)$, the distribution of grain boundary planes in commercially pure aluminum after annealing for 60 min at 400 C. The data are plotted in stereographic projection along $[001]$ and the (100) , (110) and (111) poles are marked with a circled “+”, “-” and triangle, respectively.

with tilt boundaries (perpendicular to the misorientation axis). At small misorientation angles, maxima are reached at all of the $\{111\}$ positions and at all of the positions along the zone of pure tilt boundaries. The highest points are for the (111) twist boundary and

the $\{110\}$ tilt boundaries. It should be noted that because of the discretization of the five parameter space, this plot is not selective with respect to misorientation axes and is representative of all low angle boundaries. For all of the higher angle misorientations about the $[111]$ axis, the distribution always peaks at the (111) twist position, as illustrated in Fig. 3(c) and (d). Note that the peak of nearly 28 MRD at the (111) position in $k(n|60=[111])$, usually referred to as the coherent twin, is the highest point in the five parameter distribution.

The trend that $\{111\}$ type planes are preferred is also observed for $[100]$ misorientations. For $[110]$ misorientations, on the other hand, there is no unique preferred plane. Instead, symmetric tilt boundaries are preferred at all misorientations, as illustrated in Fig. 4. For the case of $[110]$ misorientations, the common axis lies in the plane of the paper and the tilt boundaries are on the great circle perpendicular to this axis, marked by a dark line in Fig. 4(a). For misorientations up to about 50 (the Σ_{11} misorientation) the preferred boundary plane is symmetric about $[001]$. In other words, the planes bounding each of the crystals on either side of the boundary are in the zone of tilts, inclined by $\alpha/2$ from $[001]$. Beyond this angle, the preferred planes are symmetric about $[\bar{1}10]$ (see Fig. 4(d)).

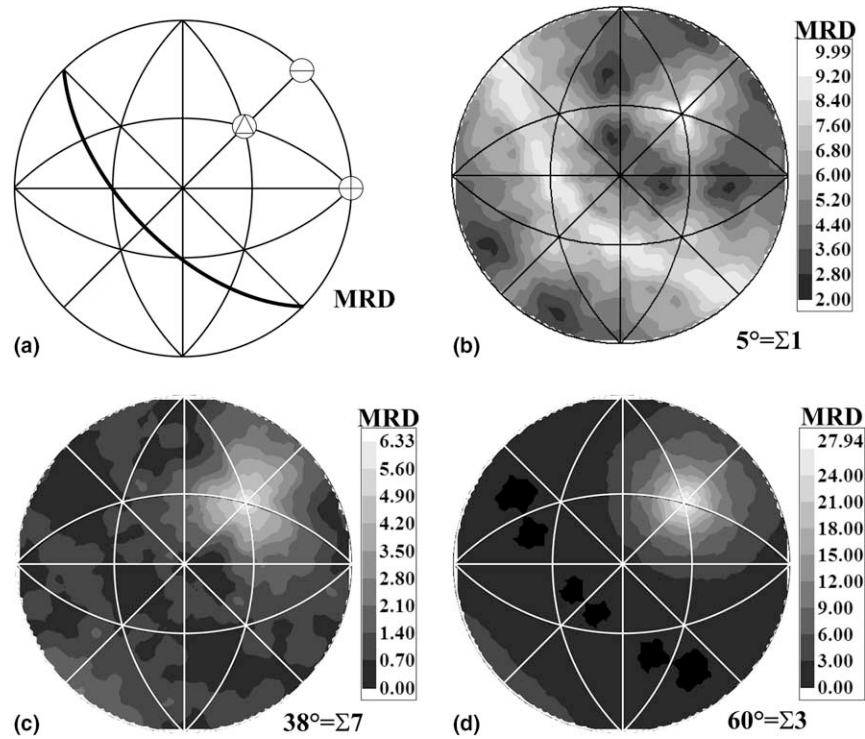


Fig. 3. Distribution of grain boundary planes for [1 1 1] misorientations. (a) Schematic of the reference frame for the [0 0 1] stereographic projections. The [1 1 1] misorientation axis is marked by the circled triangle and shows the position of twist boundaries. The positions of the tilt boundaries are shown by the dark line and the [1 0 0] and [1 1 0] directions are denoted by the circled + and -, respectively. (b) $k(n|5 = [1 1 1])$, (c) $k(n|38 = [1 1 1])$, (d) $k(n|60 = [1 1 1])$.

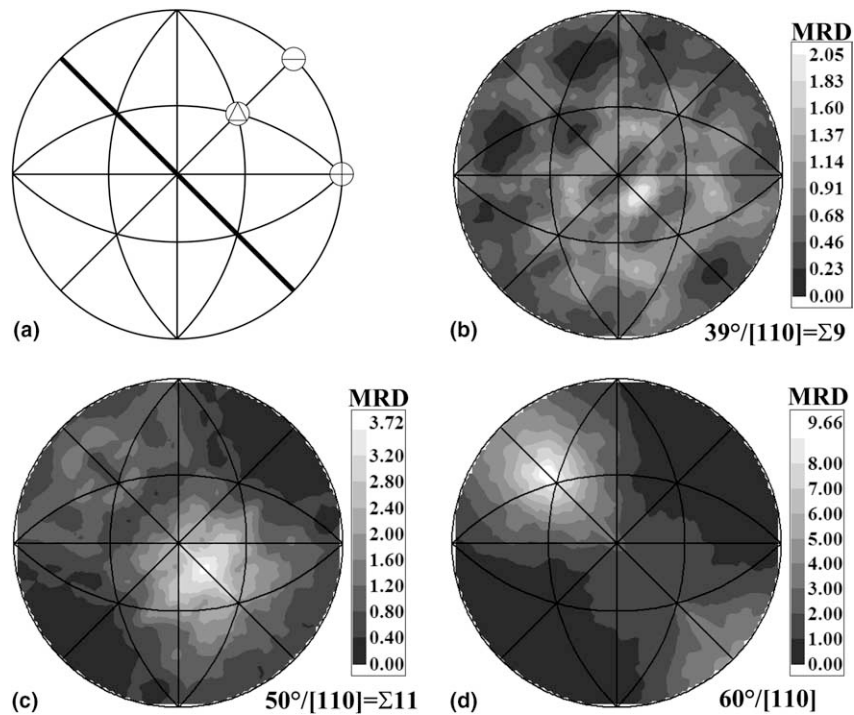


Fig. 4. Distribution of grain boundary planes for [1 1 0] misorientations. (a) Schematic of the reference frame for the [0 0 1] stereographic projections. The [1 1 0] misorientation axis is marked by the circled - and shows the position of twist boundaries. The zone of tilt boundaries is shown by the dark line. (b) $k(n|39 = [1 1 0])$, (c) $k(n|50 = [1 1 0])$, (d) $k(n|60 = [1 1 0])$.

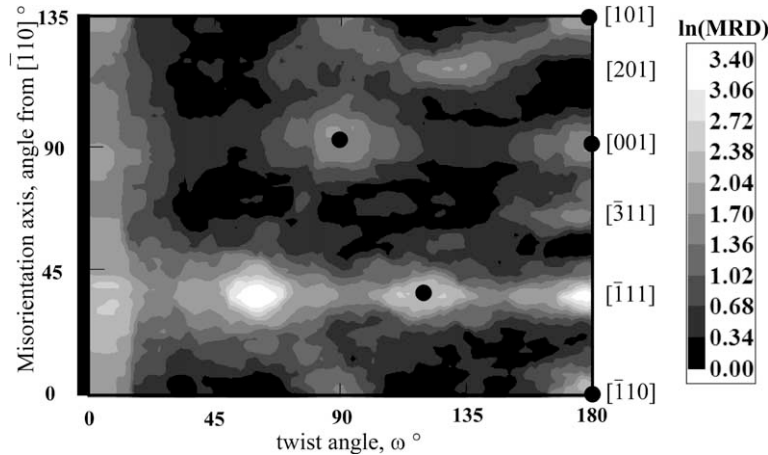


Fig. 5. Twist boundaries for all misorientation axes on the edges of the standard stereographic triangle. The far left hand side of the field and the black circles are positions of zero misorientation. Note that for $x = 180$, the line from $[1\ 1\ 0]$ to $[0\ 0\ 1]$ gives the populations of the $[1\ 1\ 0]$ symmetric tilts.

To further examine the importance of low index surfaces, we can also plot the population of twist boundaries for all axes found on the edges of the standard stereographic triangle, as illustrated in Fig. 5. Horizontal lines on this plot give the population of twist boundaries as a function of twist angle for a single misorientation axis. The high population on the left hand side is the location of low angle boundaries. Other positions of zero misorientation are marked with a black circle. The peaks for 60 and 180 twists about $[1\ 1\ 1]$ are the coherent twin illustrated in Fig. 3(d). The peak at 180 around $[3\ 1\ 1]$ is symmetrically indistinguishable from the boundary that creates the symmetric tilt boundary shown in Fig. 4(c). Other 180 twist boundaries between $[3\ 1\ 1]$ and $[0\ 0\ 1]$ also have high populations (henceforth they are referred to as $\{1\ 1\ w\}$ (twist boundaries). There is also a peak for the 135 twist about $[2\ 0\ 1]$. However, this misorientation is symmetrically indistinguishable from a misorientation in the fundamental zone that is very close to $\Sigma 3$. Therefore, the elevated population at this position occurs because the discrete boundary categories overlap at these misorientations. One overall trend in the plot is that twists about $[1\ 1\ 1]$ and $[1\ 0\ 0]$ axes generally have higher populations than those around other axes. For the $\langle 110 \rangle$ type axis, there is only a modest peak at the 90 twist configuration.

We also consider inequivalent low index twist configurations, not technically twist boundaries, but still bounded on both sides by a low index surface. For example if the $[1\ 0\ 0]$ axis of one crystal is parallel to the $[1\ 1\ 0]$ axis of its complement in the bicrystal, and the grain boundary plane is simultaneously perpendicular to both, then rotations about the common axes produce bicrystals whose boundaries always have the same low index surfaces (but not necessarily the same common axis of rotation). For the $(100)\|(110)$ configurations, the maximum is reached at about 1.7 MRD, for a rotation of 45 with respect to the common $[1\ 0\ 0]$ axis. For

boundaries with $(110)\|(111)$, the populations are consistently low, 0.4 ± 0.05 MRD. On the other hand, boundaries with $(100)\|(111)$ all have populations of 3.0 ± 0.5 MRD. Note that with the exception of $[1\ 1\ 1]$ twists, the population of $(100)\|(111)$ boundaries is higher than all other low index twists.

4. Discussion

Based on the results of earlier experimental studies and predictions from simulations, we expect that the grain boundaries with high populations are also those that have low energies [4]. Energies of $[1\ 1\ 0]$ symmetric tilt boundaries, measured by Hasson and Goux [9], are compared to the measured populations in Fig. 6. The main features of the measured energy are reproduced in

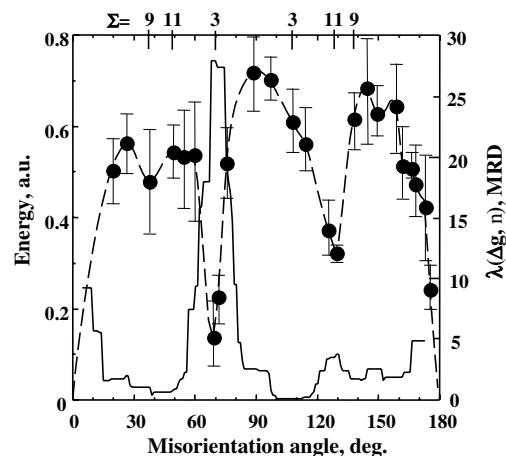


Fig. 6. Comparison of measured energies [9] (dashed line) to populations (solid line) for symmetric $[1\ 1\ 0]$ tilt boundaries. Both lines are simple interpolations between the data points. The misorientation angle is the angle between the $[1\ 1\ 0]$ directions in the two crystals.

the observed population: the population increases at small misorientation angles, at the coherent twin, $k(60 = [111], [111])$, and at the $[\bar{3}11]$ 180° twist, which is also $k(50 = [110]; [1\bar{1}3])$. Finally it should be noted that while these are $\Sigma 3$ and $\Sigma 11$ lattice misorientations, this is not the feature that distinguishes them from other boundaries. Equivalent lattice misorientations appear within the same set of symmetric tilt boundaries, but are not special in energy or population. In this case, it is the plane on which the boundary forms that distinguishes the low energy configuration from the higher energy boundaries with the same lattice misorientation.

In prior work, we observed a strong correlation between grain boundary populations and the surface energy anisotropy [2–4]. In other words, grain boundaries with low energy, low index planes correspond to local maxima in the distribution. The correlation is quite dramatic in ceramics such as MgO [4], SrTiO₃ [2], TiO₂ [3], and MgAl₂O₄ [3,10], where the surface energy anisotropy is thought to be large (>10%). In these cases, asymmetric boundaries where one of the two grains is terminated by a low index face are favored over more symmetric boundaries that would be expected to have lower energies on the basis of atomic coincidence in the grain boundary plane. A study of an Fe–Si alloy with the body centered cubic structure showed that $\{110\}$ planes occurred most frequently, but the trend was weaker than in the more anisotropic ceramic systems [11].

Studies of small cavities in aluminum have shown that the (111) surface has the lowest energy, (110) has the highest, and (100) is intermediate [12]. However, the total anisotropy is only 5%. The observation that (111) twists, (100) twists, and (100)|| (111) configurations all have populations that are larger than twist boundaries comprised of other surfaces suggests that these grain boundaries are made from surfaces that have relatively lower energies. The rationale for this behavior is that the grain boundary energy must be the sum of the energies required to create the adjoining surfaces, minus an energy that is released as the two surfaces are joined and the atoms from the adjacent crystals form bonds and relax to lower energy configurations. The latter contribution is referred to as the binding energy. Theoretical estimates of the binding energy have shown that it increases with the average interplanar spacing of the two surfaces adjoining the boundary [13,14]. Note that low energy surface planes generally have low indices, high planar densities, and, therefore, large interplanar spacings. As a result, the influence of low energy surfaces on reducing the grain boundary energy is reinforced by the higher binding energy that is usually associated with these same surfaces.

If the relative abundance of a boundary type inversely reflects the grain boundary energy, then there are also boundaries in the observed distribution that, based on the simple model described above, would not be ex-

pected to have especially low energies. For example, consider the [110] symmetric tilt boundaries, where boundaries with symmetric $\{11w\}$ boundary planes have relatively high populations. For the case of the $\Sigma 11$ misorientation, $k(n|50=[110])$, the peak is at the $[1\bar{1}3]$ position. This boundary can also be described as a 180° twist about the $[\bar{3}11]$ axis and the data in Fig. 5 illustrate that all of the 180° twists with indices $[\bar{w}11]$ have relatively high populations. Since a relatively low energy is not expected on the basis of the presumed surface energy or binding energy anisotropy, one might speculate that a special coincidence relationships within the boundary plane may increase the binding energy more than expected on the basis of the interplanar spacing and that this feature may lead to a reduced energy. We have therefore computed the planar coincident site density and compared it to the population for a number of special configurations. The results, which are tabulated in Table 1 and summarized graphically in Fig. 7, show that the planar coincident site density is not well correlated to the population. For example, the second

Table 1
Geometric data for selected grain boundaries

Δg (Σ)	n [uvw]	d_{hkl} (Å)	PCSD (atoms/a ²)	$k(\Delta g; n)$ (MRD)
3	111	0.577	2.31	27.95
3	211	0.408	0.82	0
5	100	0.500	0.4	0.51
5	210	0.224	0.89	0.49
5	310	0.158	0.63	0.54
7	111	0.577	0.33	6.34
7	321	0.134	0.18	0.01
9	110	0.354	0.16	0.25
9	221	0.167	0.67	0.90
9	411	0.118	0.47	1.68
11	110	0.354	0.13	0.30
11	332	0.107	0.43	0.75
11	311	0.302	1.21	3.71

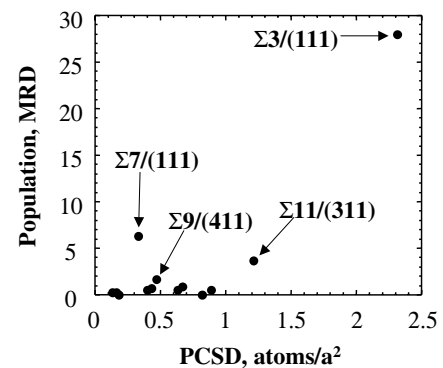


Fig. 7. Population of boundaries listed in Table 1, versus the planar coincident site density (PCSD). The four highest population boundaries are labeled.

highest population, $k(38 = [111]; [111])$, which is a $\Sigma 7$ boundary, has the fourth lowest planar coincident site density. In this case, as with the coherent twin, the high population can be correlated with the presence of (111) planes on both sides of the interface. Furthermore, the symmetric $\Sigma 5$ tilt on the (210) plane has a relatively low population, even though it has a relatively high planar coincidence. Based on these comparisons, it does not appear that planar coincidence provides a plausible explanation for the observations. This same conclusion was reached by Goodhew et al. [15] in a study of grain boundaries in gold.

Using atomistic simulations, Wolf [16] studied the relationship between grain boundary energy, boundary crystallography and cleavage energy. By calculating the energy of symmetrical tilt and twist boundaries in fcc metals, he found that: (a) the energy of random high angle grain boundaries is inversely correlated with the spacing of the terminating plane at the boundary; (b) only boundaries based on $\{111\}$ and $\{113\}$ planes exhibit unusually low energies; (c) the cleavage energy is inversely correlated with the grain boundary energy; (d) for the majority of boundaries, the grain boundary energy scales with the surface energy. These results were essentially the same regardless of whether the calculation employed a Lennard-Jones potential or an interatomic potential fitted to the properties of gold. These results are strikingly similar to the pattern observed here in grain boundary populations in aluminum. All $\{111\}$ twist boundary types are highly populated, suggesting a low relative energy. The $\Sigma 11/\{113\}$ is also highly populated, again in agreement with the low energy found in atomistic simulations. Essentially all other boundary types exhibited no unusually low energy: in the $\langle 100 \rangle$ tilt series, for example, no unusually low energy cusps were found, again in agreement with the population statistics. Because Wolf [16] did not examine boundaries with $\{100\} \parallel \{111\}$, it is not possible to compare the observed population to the energies of these boundaries. Overall, the results of the atomistic simulations point to a strong correlation between grain boundary energy and average surface energy, just as the boundary population statistics suggest.

The moderately high population of certain boundaries that are not expected to have especially low energies on the basis of their surface and binding energies, such as the $\{11w\}$ -type twists, cannot yet be easily explained. It might be that atomic reconstruction of the boundary lowers the energy more than would be ex-

pected on the basis of the trends in surface energy and binding energy. These boundaries would be interesting targets for a high resolution transmission electron microscopy study and/or further atomistic simulations.

5. Summary

The grain boundary character distribution in commercially pure aluminum is relatively isotropic. However, there is a clear tendency for grain boundaries to terminate on low index planes with relatively low surface energies and large interplanar spacings. While grain boundaries terminated by $\{111\}$ planes dominate the population, some boundaries on higher index planes such as $\{113\}$ also have populations that are higher than would be expected in a random distribution.

Acknowledgements

This work was supported primarily by the MRSEC program of the National Science Foundation under Award No. DMR-0079996.

References

- [1] Saylor DM, Morawiec A, Rohrer GS. Acta Mater 2003;51:3663.
- [2] Saylor DM, El Dasher BS, Sano T, Rohrer GS. J Am Ceram Soc 2004;87:670.
- [3] Saylor DM, El Dasher BS, Pang Y, Miller HM, Wynblatt P, Rollett AD, Rohrer GS. J Am Ceram Soc 2004;87:724.
- [4] Saylor DM, Morawiec A, Rohrer GS. Acta Mater 2003;51:3675.
- [5] Morawiec A. J Appl Crystallogr 1998;31:818.
- [6] Saylor DM, Adams BL, El Dasher BS, Rohrer GS. Met Mater Trans [in press].
- [7] Wright SI, Larsen RJ. J Micro 2002;205:245.
- [8] Frank FC. Met Trans 1998;19A:403.
- [9] Hasson GC, Goux C. Scr Metall 1971;5:889.
- [10] Miller HM, Saylor DM, El Dasher BS, Rollett AD, Rohrer GS. Crystallographic distribution of internal interfaces in spinel polycrystals. In: Second International Conference on Recrystallization and Grain Growth [in press].
- [11] Bennett TA, Kim C-S, Rohrer GS, Rollett AD. Five-parameter grain boundary character distribution in Fe-1%Si. In: Second International Conference on Recrystallization and Grain Growth [in press].
- [12] Nelson RS, Mazey DJ, Barnes RS. Philos Mag 1965;11:91.
- [13] Wolf D, Phillpot S. Mater Sci Eng A 1989;107:3.
- [14] Sutton AP. Prog Mater Sci 1992;36:167.
- [15] Goodhew PJ, Tan TY, Balluffi RW. Acta Met 1978;35:557.
- [16] Wolf D. J Mater Res 1990;5:1708.